Role of synergy and antagonism in designing multidrug adaptive chemotherapy schedules

Y. Ma[*]

Department of Physics & Astronomy, University of Southern California, Los Angeles, California 90089-1191, USA

P. K. Newton [†]

Department of Aerospace & Mechanical Engineering, Mathematics, and The Ellison Institute,
University of Southern California, Los Angeles, California 90089-1191, USA

Chemotherapeutic resistance via the mechanism of competitive release of resistant tumor cell subpopulations is a major problem associated with cancer treatments and one of the main causes of tumor recurrence. Often, chemoresistance is mitigated by using multidrug schedules (two or more combination therapies) that can act synergistically, additively, or antagonistically on the heterogeneous population of cells as they evolve. In this paper, we develop a three-component evolutionary game theory model to design two-drug adaptive schedules that mitigate chemoresistance and delay tumor recurrence in an evolving collection of tumor cells with two resistant subpopulations and one chemosensitive population that has a higher baseline fitness but is not resistant to either drug. Using the nonlinear replicator dynamical system with a payoff matrix of Prisoner's Dilemma (PD) type (enforcing a cost to resistance), we investigate the nonlinear dynamics of this three-component system along with an additional tumor growth model whose growth rate is a function of the fitness landscape of the tumor cell populations. A key parameter determines whether the two drugs interact synergistically, additively, or antagonistically. We show that *antagonistic* drug interactions generally result in slower rates of adaptation of the resistant cells than *synergistic* ones, making them more effective in combating the evolution of resistance. We then design *evolutionary cycles* (closed loops) in the three-component phase space by shaping the fitness landscape of the cell populations (i.e., altering the evolutionary stable states of the game) using appropriately designed time-dependent schedules (adaptive therapy), altering the dosages and timing of the two drugs. We describe two key bifurcations associated with our drug interaction parameter which help explain why antagonistic interactions are more effective at controlling competitive release of the resistant population than synergistic interactions in the context of an evolving tumor.

I. INTRODUCTION

We study a mathematical model to explore the role of synergisitic versus antagonistic multidrug interactions on an evolving population of cancer cells in a tumor. Building on our single drug, single resistant cell population adaptive therapy model developed in Ref. [1], we develop a more complex model in which we have the ability to independently administer two drugs to a coevolving population of chemosensitive cells, and two resistant populations. Using an evolutionary game theory approach, we model how these populations respond to the drug schedules as they coevolve. The model includes a separate tumor growth equation which tracks the total tumor volume with a growth rate that is a function of the fitness landscape defined by the subpopulations of cancer cells. Developed in the same spirit as Ref. [1], our deterministic model is purposely simple enough to extract several key features associated with antagonistic, synergistic, or additive multidrug interactions, with a parameter that we use to adjust these interactions.

There is a large and dedicated literature on characterizing the interactions of many different multidrug combinations of toxins on static cell populations. As far as we are aware, the first comprehensive study of synergistic versus antagonistic effects was carried out by Bliss [2] in 1939, using joint probabilities, leading to a formula that is commonly called the Bliss index for drug interactions. A similar but slightly modified criterion was introduced by Loewe [3] and more recently developed further by Chou and collaborators [4]. These indices have all been used to help quantify the many different types of interactions that can occur with two or more toxins applied jointly in a static population of cells. In this context, it is common to assume that synergistic interactions are desirable in most circumstances, as a lower total dosage accomplishes the same kill rate as a higher dose would accomplish if the drugs acted independently. These kinds of studies have been used effectively to choose appropriate drug cocktails to individual patients by testing wide ranges of combinations on tissue samples obtained from patient tumors [5].

When the interacting population of cells are evolving, however, the relevant effectiveness criteria become more complex. This is due to the fact that the subpopulations of cells respond differently to the different toxins applied, and as they respond, an ever-changing (adaptive) combination of toxins might be required to accomplish a given goal. Instead of

———————
[*]yongqiam@usc.edu
[†]Corresponding author: newton@usc.edu

necessarily killing the maximum number of cancer cells with the least amount of toxin, it is often the case that the goal becomes avoiding chemoresistance and delaying unwelcome tumor recurrence to the maximum extent possible. A strategy called *resistance management* [6] is often advocated and occasionally implemented [7]. These kinds of strategies have been advocated and implemented in chemotherapy settings [8–14], but perhaps have been most elegantly and thoroughly carried out in a bacterial setting (since experiments are more practical) by Kishony and collaborators [15–20] who even discuss strategies that might reverse antibiotic resistance [19]. See also Ref. [21] for recent work discussing both microbial populations and cancer cells and Refs. [22,23] for novel sequential therapy methods. In the context of evolving microbial populations [24], mutations occur frequently and it is important to consider not only pre-existing mutated subpopulations, but also mutations that occur as a result of the application of antibiotic agents. In the case of chemotherapeutic resistance in tumors, it is often assumed that resistant mutations occurred before the application of treatment, hence it is common to separate the subpopulations into sensitive and resistant subpopulations, with resistant subtypes, as we do in our deterministic model which does not include further mutations during treatment. See Ref. [25] for further discussions of these and related issues, and see Refs. [26,27] for discussions of the general approach of using evolutionary game theory in biology.

More specifically, our model is based on a replicator dynamical system of three (well-mixed) populations of cells: (i) sensitive cancer cells, S, that are sensitive to both drug 1 and drug 2, (ii) a resistant population, R_1, that is sensitive to drug 1 but resistant to drug 2, and (iii) resistant population, R_2, that is sensitive to drug 2 but resistant to drug 1. In contrast to our single-drug model developed in Ref. [1] which used one control function to administer the dose, the drug dosing schedules are administered by our two time-dependent control functions $C_1(t)$, and $C_2(t)$ that represent the chemotherapy dosing. We constrain these functions to lie in the range of values $0 \leqslant C_1 \leqslant 1$, $0 \leqslant C_2 \leqslant 1$ (with a total dose upper threshold $C_1 + C_2 \leqslant 1$). We use these control functions to shape the fitness landscape of the coevolving populations to manage resistance.

The replicator dynamical system governing the relative frequencies of (S, R_1, R_2) makes use of a 3×3 payoff matrix A of Prisoner's Dilemma type [1,28–31] which implements a cost of resistance fitness penalty for the resistant populations [32]. Our general goal is to design adaptive multidrug chemotherapy schedules that delay tumor recurrence (regrowth) due to competitive release of the resistant cell population [8,33–35] and to quantify the role of synergistic and antagonistic drug interactions in this process.

In Sec. II we introduce the details of the three-component replicator dynamical system that we use to simulate multidrug adaptive chemotherapy schedules, along with the coupled tumor growth equation. Section III describes the effects of constant chemotherapy schedules on the coevolving populations, along with our parameter e over a range of positive (synergistic) to negative (antagonistic) values. We describe in detail the transcritical bifurcations that occur and the tumor growth in response to the chemotoxins. In Sec. IV we

introduce adaptive time-dependent schedules $[C_1(t), C_2(t)]$ along with the parameter e with the goal of delaying tumor recurrence and we discuss the rate of adaptation of the cell populations in this context. Finally in Sec. V we discuss the relevance of our model to the design of adaptive-therapy clinical trials.

II. A THREE-COMPONENT REPLICATOR SYSTEM

A. The three-component model

The model we employ is a three-component replicator dynamical system for three subpopulations of cells: $(S, R_1, R_2) \equiv (x_1, x_2, x_3)$

$$\dot{x}_1 = (f_1 - \langle f \rangle)x_1, \tag{1}$$

$$\dot{x}_2 = (f_2 - \langle f \rangle)x_2, \tag{2}$$

$$\dot{x}_3 = (f_3 - \langle f \rangle)x_3, \tag{3}$$

where each dependent variable represents the relative frequencies of cells, with $x_1 + x_2 + x_3 = 1$. In these equations, f_i represents the fitness of subpopulation $i = 1, 2, 3$, while $\langle f \rangle$ represents the average fitness of all three subpopulations. These equations then give rise to the obvious interpretation that if a given subpopulation's fitness is above(below) the average, it grows(decays) exponentially - reproductive prowess is directly associated with the deviation of the fitness of a subpopulation from the average fitness of the entire population.

The fitness functions are frequency-dependent (i.e., nonconstant), which couples Eqs. (1)–(3) nonlinearly. The subpopulation fitness f_i ($i = 1, 2, 3$) function is given by

$$f_i = 1 - w_i + w_i(A\vec{x})_i, \tag{4}$$

$$A = \begin{bmatrix} a_{11} & a_{12} & a_{13} \\ a_{21} & a_{22} & a_{23} \\ a_{31} & a_{32} & a_{33} \end{bmatrix}, \tag{5}$$

where A is a 3×3 payoff matrix which introduces the evolutionary game being played by x_1, x_2, and x_3. In this paradigm, the sensitive population (x_1) are the defectors (higher fitness) and both groups of resistant cells (x_2 and x_3) are the cooperators (lower, but not equal fitness). As in Ref. [1], we use $0 \leqslant w_i \leqslant 1$ as a time-dependent parameter to administer the dose, which determines the relative strength of selection in the system. When $w_i \sim 0$, selection is relatively weak and the evolutionary game does not play a big role in the balance of the three subpopulations. When $w_i \sim 1$, selection is strong, and the game plays a bigger role. Both of those limiting cases have been discussed in the literature [36,37] for the case of finite cell population models (i.e., Moran processes), since it is easy to show that any constant parameter w_i can be scaled out of the deterministic system. For the case of time-dependent chemotherapy schedules, however, it cannot be scaled out, and we use the selection parameter $w_i(t)$ as our mechanism to introduce chemotherapy schedules to design a favorable fitness landscape for our system. The relative fitness of the three subpopulations
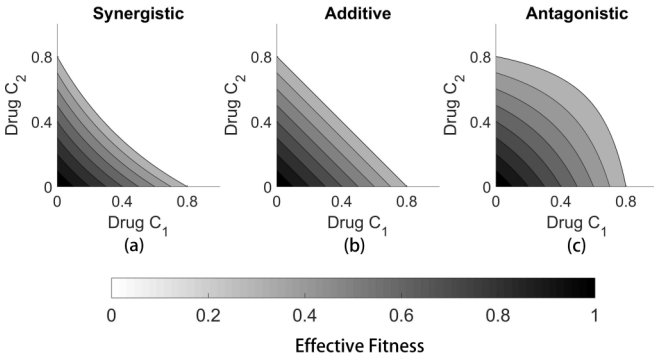
FIG. 1. (a) $e > 0$ showing synergistic profiles; (b) $e = 0$ showing additive profiles; (c) $e < 0$ showing antagonistic profiles.

are given by

$$w_1 = w_0[1 - C_1(t) - C_2(t) - eC_1(t)C_2(t)], \quad (6)$$

$$w_2 = w_0[1 - C_1(t)], \quad (7)$$

$$w_3 = w_0[1 - C_2(t)], \quad (8)$$

where w_0 is a constant that simply scales time (we take $w_0 = 0.1$). A key difference between the model developed in Ref. [1] and our model here is the fitness function Eq. (6), which gives us the ability to create synergy and antagonistic interactions by varying the parameter e. Specifically, when $e > 0$, the drugs interact synergistically, when $e = 0$, the drugs are additive, and when $e < 0$, they interact antagonistically. Level curves of the fitness profiles as a function of C_1 and C_2 are shown in Fig. 1 which can be compared with Fig. 1 of Ref. [15]. In the neutral case, additive drug interactions [Fig. 1(b)] accomplish exactly the kill rate that the sum of each of the two would accomplish acting independently. By contrast, synergistic drug interactions [Fig. 1(a)] bend the curves inward, indicating that the growth rates (fitness) are lowered more than the two dosages would accomplish independently, while antagonistic interactions [Fig. 1(c)] bend the curves outward, indicating that the growth rates are lowered less than the two dosages would accomplish independently.

To introduce a tumor growth equation, we need the equation for the average fitness of the population, given by

$$\langle f \rangle = f_1 x_1 + f_2 x_2 + f_3 x_3. \quad (9)$$

The condition for the payoff matrix A to be of (PD) type is

$$a_{21} < a_{11} < a_{22} < a_{12}, \quad (10)$$

$$a_{31} < a_{11} < a_{33} < a_{13}, \quad (11)$$

$$a_{32} < a_{22} < a_{33} < a_{23}, \quad (12)$$

and for definiteness, we choose the specific values:

$$A = \begin{bmatrix} 2 & 2.8 & 2.8 \\ 1.5 & 2.1 & 2.3 \\ 1.5 & 1.8 & 2.2 \end{bmatrix}. \quad (13)$$

For the static game, it is easy to show that the cancerous state $(S, R_1, R_2) = (x_1, x_2, x_3) = (1, 0, 0) \equiv \mathbf{p}^{*T}$ is a strict Nash
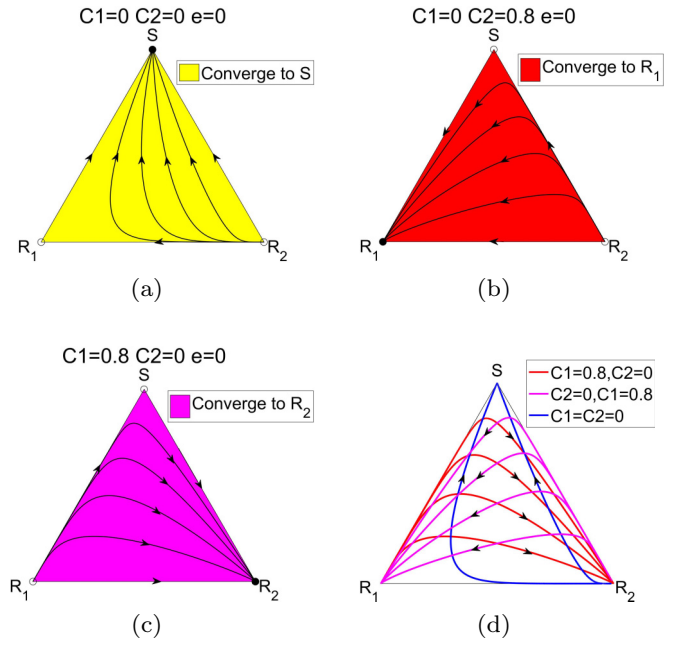

FIG. 2. Depiction of evolutionary stable states (ESS) for different chemotherapy values. (a) With no chemotherapy, the tumor saturates to the S corner regardless of the initial make-up of the three subpopulations. (b) With $C_1 = 0$, and $C_2 = 0.8$, competitive release of the resistant population R_1 drives all trajectories to the R_1 corner. (c) With $C_1 = 0.8$ and $C_2 = 0$, competitive release of the resistant population R_2 drives all trajectories to the R_2 corner. (d) Trajectories associated with three different constant combinations of C_1 and C_2, depicting the overlap of the trajectories at different times.

equilibrium in the absence of chemotherapy ($C_1 = 0, C_2 = 0$) and an ESS for the replicator system, as shown in the diagram of Fig. 2(a) where the entire triangular region is the basin of attraction for the S population.

A separate important ingredient in our model, which was not needed in our simpler single-drug model developed in Ref. [1], is our tumor-growth equation for tumor volume, which we denote $x_{\text{tumor}}(t)$:

$$\dot{x}_{\text{tumor}} = (\langle f \rangle - g)x_{\text{tumor}}, \quad (14)$$

where the growth (decay) of the tumor is a function of the average fitness associated with the tumor minus a constant background fitness level g, associated with the surrounding tissue (say, healthy cells) and microenvironment [38]. When the average fitness level of the population of cancer cells is higher than g (we take $g = 1.05$ in our simulations), the tumor grows, and when it is lower, the tumor regresses. Our chemotherapy schedules $C_1(t)$ and $C_2(t)$ largely control this complex dynamic by modifying the Nash equilibria and ESS's of the system via the fitness function Eq. (4).

B. Why the prisoner's dilemma game?

It is useful to briefly step back from our more complex three-component model Eqs. (1)–(3) to understand why, exactly, the prisoner's dilemma (PD) payoff matrix is used for modeling coevolving tumor cell populations. Consider, more simply, a reduced two-component system with a population of

healthy cells H, and a population of sensitive cancer cells S, each competing for the best payoffs. The standard version of the prisoner's dilemma payoff matrix is

$$\hat{A} = \begin{bmatrix} a & b \\ c & d \end{bmatrix} = \begin{bmatrix} 3 & 0 \\ 5 & 1 \end{bmatrix}, \tag{15}$$

where the healthy cells are the cooperators, and the cancer cells are the defectors [31]. Unlike other contexts in which game theory is used, cells are not making strategic decisions, instead, their strategy is encoded in their reproductive prowess, and selection is frequency dependent. In any mixed population $\vec{x} = (x_H, x_S)^T$, $0 \leqslant x_H \leqslant 1$; $0 \leqslant x_S \leqslant 1$; $x_H + x_S = 1$, the fitness functions, $\vec{f} = (f_H, f_S)^T$, associated with the two subpopulations are

$$\vec{f} = \hat{A}\vec{x}, \tag{16}$$

which in component form yields

$$f_H = (\hat{A}\vec{x})_1 = 3x_H + 0x_S, \tag{17}$$

$$f_S = (\hat{A}\vec{x})_2 = 5x_H + 1x_S, \tag{18}$$

while the average fitness of the total population is given by the quadratic form:

$$\langle f \rangle = \vec{x}^T \hat{A}\vec{x} = 3x_H^2 + 5x_H x_S + x_S^2 \geqslant 1. \tag{19}$$

The average fitness of the healthy state $(x_H, x_S) = (1, 0)$ is given by $\langle f \rangle|_{(x_H=1)} = 3$, while that of the cancerous state $(x_H, x_S) = (0, 1)$ is given by $\langle f \rangle|_{(x_S=1)} = 1$, which minimizes the average fitness. For the static game, the cancerous state $(x_H, x_S) = (0, 1) \equiv \mathbf{p}^{*T}$ is a strict Nash equilibrium since $\mathbf{p}^{*T} A \mathbf{p}^* > \mathbf{p}^T \hat{A} \mathbf{p}^*$, for all $\mathbf{p}$ [28]. We can then embed this static game into an evolutionary context using the replicator dynamical system [29]:

$$\dot{x}_H = (f_H - \langle f \rangle)x_H, \tag{20}$$

$$\dot{x}_S = (f_S - \langle f \rangle)x_S, \tag{21}$$

from which [using values from Eq. (15)] it is straightforward to show

$$\dot{x}_S = x_S(f_S - \langle f \rangle) = x_S(1 - x_S)(2 - x_S), \tag{22}$$

with fixed points at $x_S = 0, 1, 2$. The cancerous state ($x_S = 1$) then becomes an asymptotically stable fixed point of the dynamical system Eq. (22) and an evolutionary stable state (ESS) of the system Eqs. (20) and (21), which serves to drive the system to the strict Nash equilibrium under the flow. The fact that this ESS also corresponds to the one with the lowest average fitness is an extra feature of the PD game. For any initial condition containing at least one cancer cell, $0 < x_S(0) \leqslant 1$, we have

(i) $x_S \to 1$, $x_H \to 0$ as $t \to \infty$,
(ii) $\langle f \rangle \to 1$ as $t \to \infty$.

The first condition (and the structure of the nonlinear equations) guarantees that the cancer cell population will saturate at the carrying capacity of 1 in an S-shaped (logistic) growth curve, while the second guarantees that this asymptotically stable carrying capacity is suboptimal, since $\langle f \rangle|_{(x_S=1)} < \langle f \rangle|_{(x_H=1)}$. For these two reasons, the prisoner's dilemma evolutionary game serves as a simple paradigm for
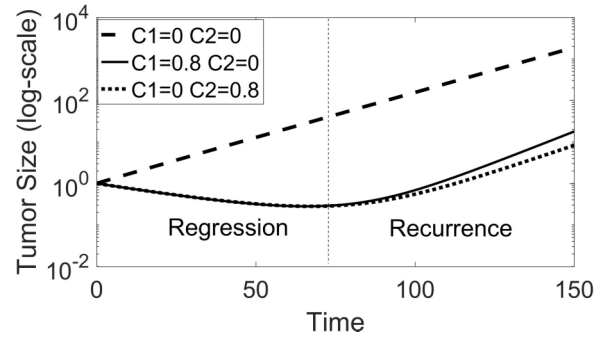

FIG. 3. Tumor growth curves (log-plots) for untreated and constant therapies. Tumor recurrence (vertical dashed line) occurs at $t \sim 75$ dimensionless time units. For these simulations we take $g = 1.05$.

tumor growth both in finite population models, as well as replicator system (infinite population) models [12,31,39,40]. This two-component system alone, however, is not able to account for the evolution of resistance, or the complexity associated with multidrug interactions which we turn to next.

III. CONSTANT CHEMOTHERAPY SCHEDULES

First, we examine the dynamical system Eqs. (1)–(3) for different constant levels of the chemoparameters C_1, C_2 ($0 \leqslant C_1 \leqslant 1$; $0 \leqslant C_2 \leqslant 1$; $C_1 + C_2 \leqslant 1$) in the case of additive $e = 0$ interactions, synergistic ($e > 0$) interactions, and antagonistic ($e < 0$) interactions.

A. Additive interactions $e = 0$

Figure 2 shows the panel of trajectories for three different scenarios. To start, Fig. 2(a) shows the trajectories with no chemotherapy—all trajectories lead to the S corner which saturates the tumor. In these figures, solid circles denote the ESS states, while open circles denote the unstable states. Figure 2(b) shows trajectories with $C_1 = 0$, $C_2 = 0.8$. In this case, competitive release of the R_1 population allows it to take over the tumor, with all trajectories leading to the R_1 corner. For these parameter values, R_1 is the ESS (and strict Nash equilibrium) of the system. Figure 2(c) with $C_1 = 0.8$, $C_2 = 0$ depicts competitive release of the R_2 population, with all trajectories leading to the R_2 corner, showing that R_2 is the ESS of the system.

In Fig. 2(d) we plot three different constant therapy schedules together, showing how they can intersect at different times. This gives the possibility of switching the therapies off and on at the intersection times to create a trajectory that stays in a closed loop and never reaches any of the corners—these closed loops, which we call evolutionary cycles [13], represent scenarios in which the three subpopulations stay in perpetual competition, guided by a time-dependent schedule that shapes the fitness landscapes in such a way as to manage chemotherapeutic resistance. We will describe the systematic construction of these closed loops in Sec. IV. Figure 3 shows the tumor size [using Eq. (14)] plotted logarithmically. The untreated tumor ($C_1 = 0$, $C_2 = 0$) grows exponentially, while each of the treated tumors initially show tumor regression up until $t \sim 75$, then tumor recurrence due to chemotherapeutic
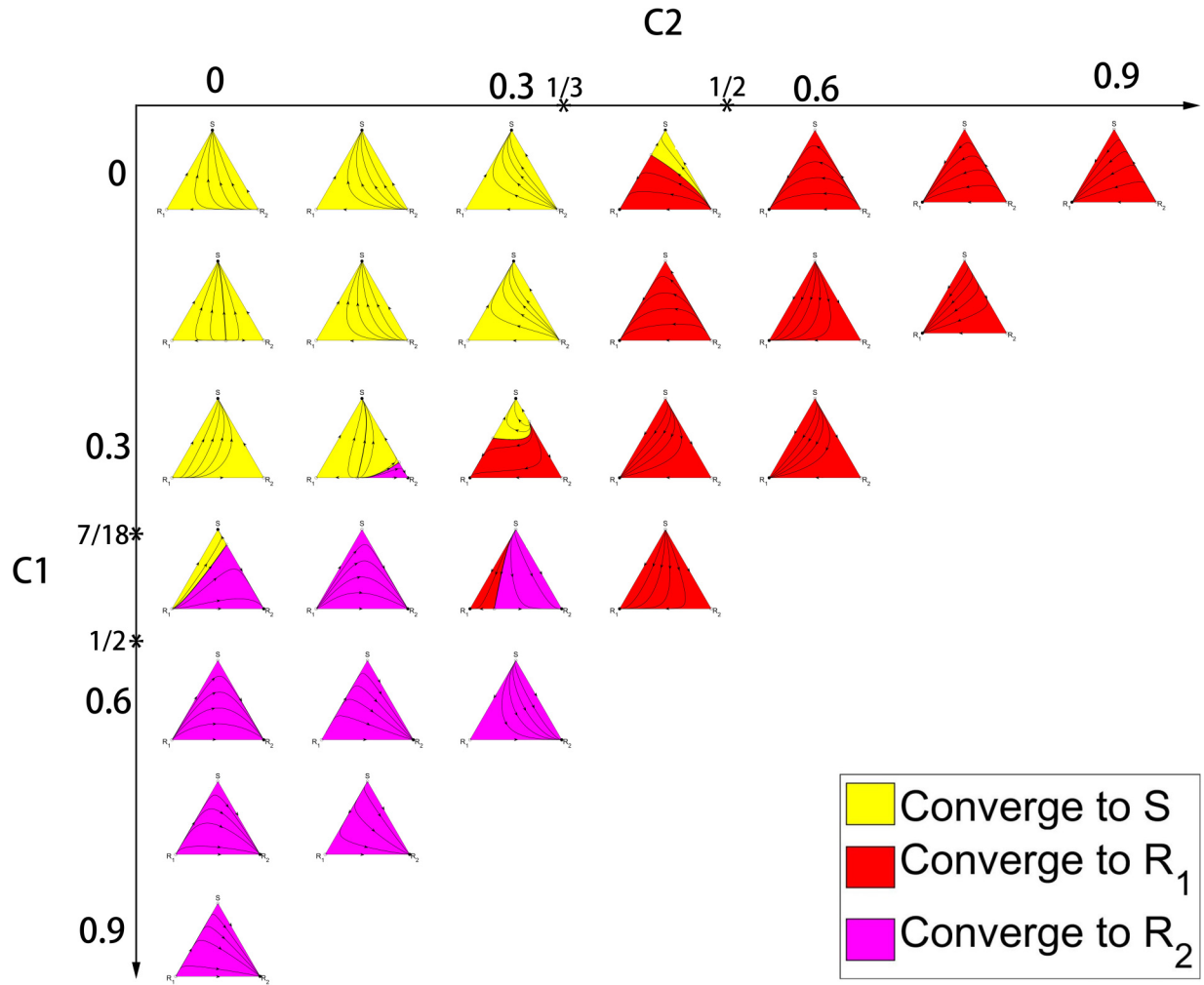
FIG. 4. Panel showing the full range of trajectories, ESS, and their basins of attraction for constant additive ($e = 0$) therapies in the range $0 \leqslant C_1 \leqslant 1, 0 \leqslant C_2 \leqslant 1, C_1 + C_2 \leqslant 1$. Bifurcation values along top row ($C_1 = 0$) are $C_2 = 1/3, C_2 = 1/2$. Bifurcation values down left column ($C_2 = 0$) are $C_1 = 7/18, C_1 = 1/2$.

resistance (either of the R_1 or R_2 populations), an unwelcome common scenario. This scenario is clearly depicted in prostate cancer data sets shown in Ref. [41] and widely discussed in the clinical literature. Our goal is to show how specially designed adaptive multidrug chemotherapies can push the tumor recurrence point further to the right on these plots.

The full range of possible constant chemotherapy profiles are shown in Fig. 4. For certain ranges of chemodosing, there are mixed basins of attraction to each of the corners, hence multiple evolutionary stable states of the system. In the top row, with $C_1 = 0$, the two critical values where the ESS's bifurcate are $C_2 = 1/3$ (R_1 changes from unstable to stable via a transcritical bifurcation) and $C_2 = 1/2$ (S changes from stable to unstable via a transcritical bifurcation). In the left column, with $C_2 = 0$, the two critical values where the ESS's bifurcate are $C_1 = 7/18$ (R_2 changes from unstable to stable via a transcritical bifurcation) and $C_2 = 1/2$ (S changes from stable to unstable via a transcritical bifurcation). This panel shows the complexity associated with the stability and basins of attraction of the three tumor subpopulations even in such a simple model, but also gives us the ability to exploit the inherent underlying dynamics associated with the

different trajectories using piecewise constant chemodosing protocols.

B. Synergistic and antagonistic interactions

Using the panel in Fig. 4 as our guide, we focus in more detail on the values $C_1 = 0.35, C_2 = 0.27$, comparing the effects of synergistic interactions and antagonistic interactions with values $-0.4 \leqslant e \leqslant 0.4$ in Fig. 5. For strongly antagonistic interactions ($e = -0.4, -0.3, -0.2$), only the two subpopulations S and R_2 compete for dominance (both ESS), with the R_1 population being an unstable state with no basin of attraction since this value of C_1 is high enough to control the R_1 population. For strongly synergistic interactions ($e = 0.2, 0.3, 0.4$), the two subpopulations R_1 and R_2 compete for dominance (both ESS), with the population of cells S sensitive to both drugs being an unstable state. In this regime, the synergistic interactions enhance the competitive release of both of the resistant subpopulations. It is the intermediate regime $e = -0.1, 0, 0.1$ that is the most interesting, and has all three evolutionary stable populations competing for dominance (all three ESS) with intertwined basins of attraction for each.
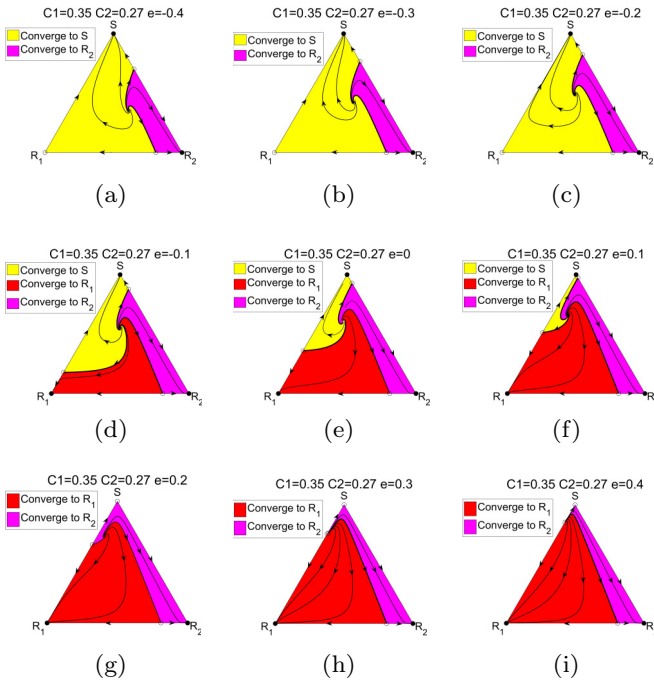
FIG. 5. The effect of synergy ($e > 0$) vs antagonism ($e < 0$) on the ESS and the basins of attraction for a fixed choice of constant combination therapies $C_1 = 0.35$, $C_2 = 0.27$. (a) $e = -0.4$; (b) $e = -0.3$; (c) $e = -0.2$; (d) $e = -0.1$; (e) $e = 0$; (f) $e = 0.1$; (g) $e = 0.2$; (h) $e = 0.3$; (i) $e = 0.4$.

Which of the subpopulations eventually wins depends very much on our initial mixture of cell types, and exactly how the two drugs interact. We examine these details next, and describe a bifurcation that occurs between the two-species coexistence and three-species coexisting states.

Transcritical bifurcations

To better understand the details of the delicate nonlinear dynamical processes that take place with antagonistic drug interactions, in Fig. 6 we focus on the range of antagonistic values $e = -0.21, -0.19, -0.175, -0.15$ for fixed values of $C_1 = 0.35$ and $C_2 = 0.27$. The relevant bifurcation that occurs at the critical value $e_c^{(a)} = -310/1701 = -0.1822$ takes place at the R_1 corner, when the fixed point $R_1 = 1$ goes from unstable ($e < e_c^{(a)}$) to asymptotically stable ($e > e_c^{(a)}$) in a transcritical bifurcation (exchange of stability). Through the bifurcation point, a stable fixed point (shown in Fig. 6(a) outside the triangle below R_1) moves up the $R_1 - S$ side of the triangle ($R_2 = 0$), and exchanges stability with the fixed point at the R_1 corner. The key point here is that when the antagonistic interaction becomes sufficiently weak, suddenly there are regions that allow for the R_1 population to saturate the tumor via competitive release. In Fig. 7 we show the details of the collision of eigenvalues that takes place [Fig. 7(a)] and the process in the dS/dt versus S plane [Figs. 7(b)–7(e)]. Figure 7(b) shows the classic transcritical bifurcation diagram (see Ref. [42]). When the level of antagonism is sufficiently large, there are only the two evolutionary stable states S and R_2.
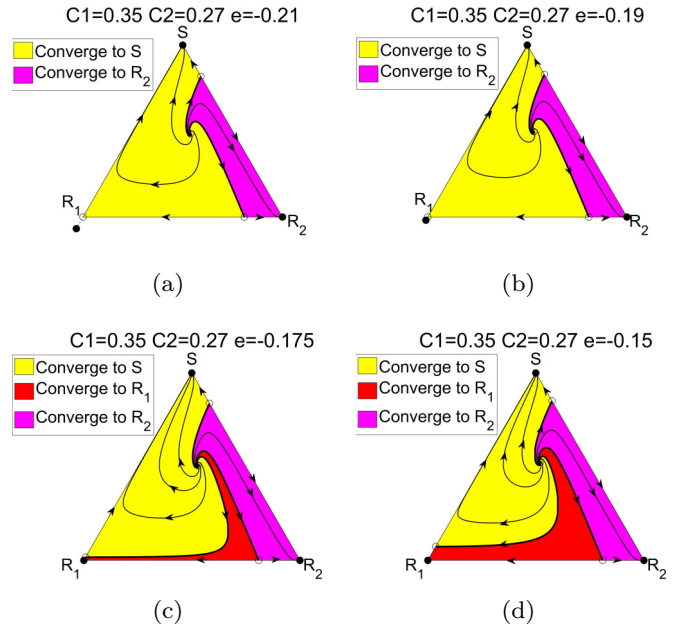

FIG. 6. The opening of the basin of attraction for R_1 via a transcritical bifurcation at $e = -310/1701 = -0.1822$, $C_1 = 0.35$, $C_2 = 0.27$. At the bifurcation point, the areas of the basins of attraction of the respective regions are $S = 76.2\%$, $R_2 = 13.8\%$. (a) $e = -0.21$; (b) $e = -0.19$; (c) $e = -0.175$; (d) $e = -0.15$.

In Fig. 8 we highlight the bifurcation that takes place in the synergistic regime around values $e = 0, 0.1, 0.2, 0.3$ for fixed values of $C_1 = 0.35$ and $C_2 = 0.27$. When synergistic interactions are sufficiently strong [Fig. 8(c)], the basin of attraction associated with the S population vanishes in a transcritical bifurcation that occurs at the critical value $e_c^{(s)} = 30/189 = 0.1587$. This is shown at the S corner, when the fixed point $S = 1$ goes from unstable ($e > e_c^{(s)}$) to asymptotically
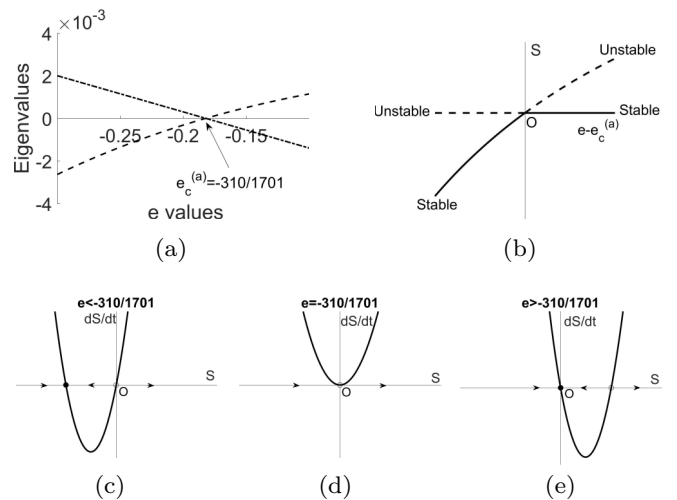

FIG. 7. Four ways of depicting the antagonistic transcritical bifurcation. (a) Eigenvalue collision that takes place as the two fixed points collide at the R_1 corner. The other eigenvalue remains negative for both fixed points; (b) transcritical bifurcation diagram; (c) prebifurcation phase plane; (d) bifurcation phase plane; (e) postbifurcation phase plane.
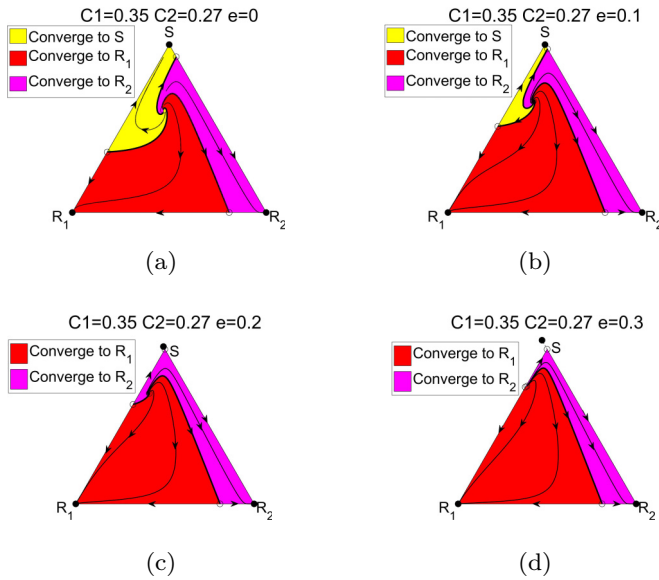
FIG. 8. The closing of the basin of attraction for S via a transcritical bifurcation at $e = 30/189 = 0.1587$, $C_1 = 0.35$, $C_2 = 0.27$. At the bifurcation point, the areas of the basins of attraction of the respective regions are $R_1 = 72.3\%$, $R_2 = 17.7\%$. (a) $e = 0$; (b) $e = 0.1$; (c) $e = 0.2$; (d) $e = 0.3$.

stable ($e < e_c^{(s)}$). The two resistant subpopulations are the only remaining evolutionarily stable states for strong synergistic multidrug interactions. The transcritical bifurcation diagram is similar to that shown in Fig. 7 so we do not repeat it.

In Fig. 9 we show the areas of three basins of attraction through the full range of values $-0.3 \leqslant e \leqslant 0.3$. The basin areas begin to rapidly change in the antagonistic regime at $e = -0.2$ and, in general, show much more sensitivity to changes in e in the antogonistic regime than the synergistic regime. The ability to make delicate and more nuanced changes in the balance of populations is strongest for interaction parameter $e \sim -0.1$ when all three basin boundaries occupy similar areas.

Figure 10 shows the average fitness curves [Fig. 10(a)] and tumor growth curves [Fig. 10(b)] through a range of values of
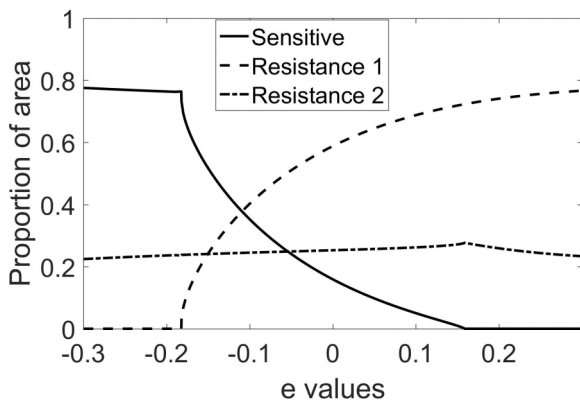

FIG. 9. Areas of the three basins of attraction as a function of the parameter e. Note the sensitivity of the S and R_1 regions in the antagonistic regime $-0.2 \leqslant e \leqslant -0.1$.
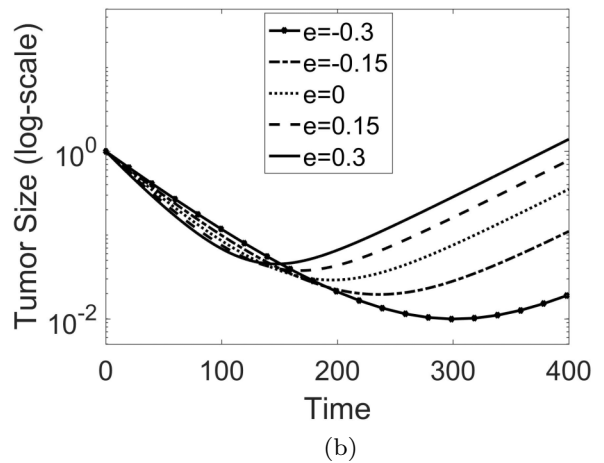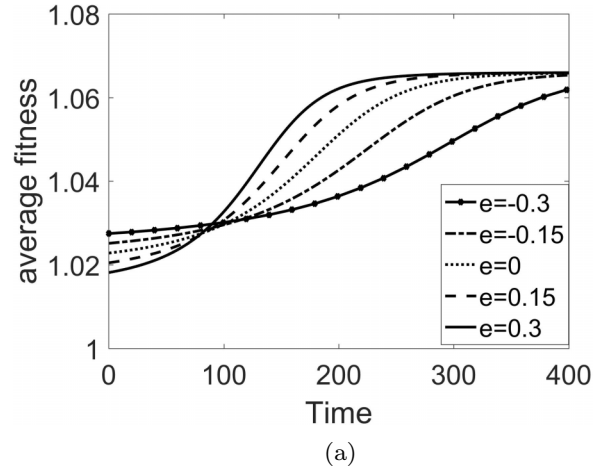

FIG. 10. (a) Average fitness curves for $e = 0.3, 0.15, 0, -0.15, -0.3$; (b) Tumor growth curves (log-plot) for $e = 0.3, 0.15, 0, -0.15, -0.3$.

e. Notice, for early times, the average fitness of the antagonistic case $e = -0.3$ is higher, but ends up lower as the system evolves. The tumor growth curve in this case follows the same trend—initially tumor growth is highest for antagonistic interactions, but it finishes lowest. Most importantly, notice that the tumor recurrence time for the antagonistic case is also pushed later in time ($t \sim 300$) showing the superiority of antagonistic drug interactions over synergistic ones in terms of managing resistance.

IV. DESIGNING ADAPTIVE EVOLUTIONARY CYCLES

Many new possibilities can be created using time-dependent chemoschedules $C_1(t)$, $C_2(t)$, if we monitor the balance of the subpopulations and adaptively make changes at judiciously chosen time points. The basic idea is shown in Fig. 2(d), where we see how the trajectories associated with different constant chemotherapy schedules cross. At any of the crossing times, it is possible to switch from one trajectory to another by switching the values of C_1 or C_2 at those crossing times as a form of control theory [43]. This basic procedure allows us to design schedules that take us from any point A in the triangle to any other point B along the legs of a path that
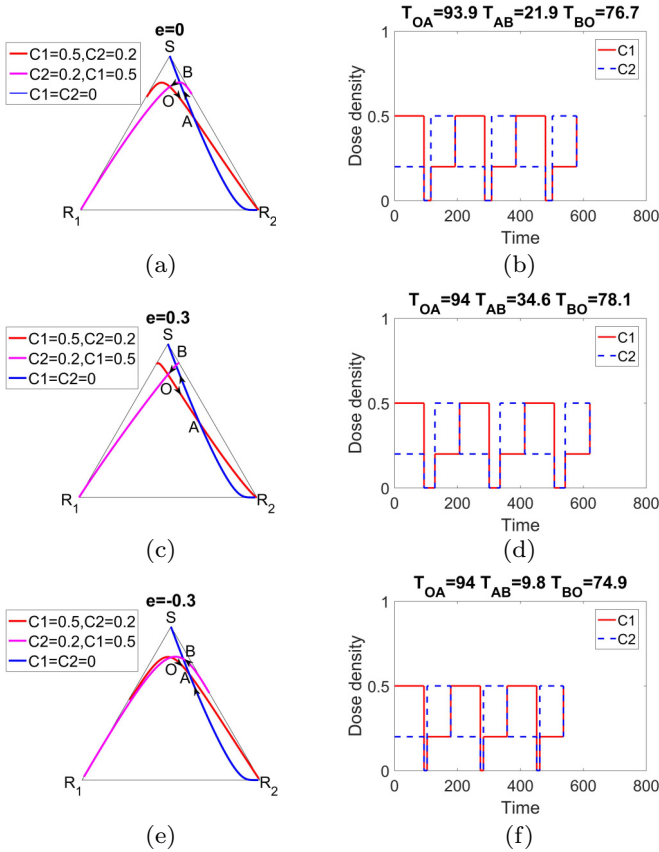
FIG. 11. Closed loop adaptive schedules *OABO* using three cycles for $e = 0, 0.3, -0.3$. (a) $e = 0$, *OA*: $C_1 = 0.5, C_2 = 0.2$, *AB*: $C_1 = 0, C_2 = 0$, *BO*: $C_1 = 0.2, C_2 = 0.5$; (b) corresponding adaptive schedule; (c) $e = 0.3$, *OA*: $C_1 = 0.5, C_2 = 0.2$, *AB*: $C_1 = 0, C_2 = 0$, *BO*: $C_1 = 0.2, C_2 = 0.5$; (d) corresponding adaptive schedule; (e) $e = -0.3$, *OA*: $C_1 = 0.5, C_2 = 0.2$, *AB*: $C_1 = 0, C_2 = 0$, *BO*: $C_1 = 0.2, C_2 = 0.5$; (f) corresponding adaptive schedule.

are separated by the switching times. Using multiple time-switching, we can also design trajectories that form closed loops, called evolutionary cycles [13] that never converge to any of the corners. This method of control was pioneered by Marsden and coworkers [44] in the context of satellite orbit design, and is also used in Ref. [1].

Figure 11 shows examples of how closed (piecewise differentiable) orbits are designed in practice. More discussion of the design of these adaptive schedules, as well as discussion of their robustness, can be found in Ref. [1] in the context of the single-drug model. In each of the figures, point O is fixed, as is the untreated (blue) curve with $C_1 = 0, C_2 = 0$. Consider the loop OABO created Fig. 11(a), with additive interaction parameter $e = 0$. In traversing the OA leg, we use $C_1 = 0.5$, $C_2 = 0.2$. When the trajectory reaches point A, we switch to $C_1 = 0, C_2 = 0$, i.e., no therapy. When we reach point B, we switch to $C_1 = 0.2, C_2 = 0.5$ until we reach point O, and then we start the schedule again to traverse the same loop as many times as we desire. The dose density plot is shown in Fig. 11(b). Figures 11(c) and 11(d) use the same dosing values, but with $e = 0.3$ (synergistic). The loop in this case is larger (encloses more area), so there is a larger deviation in the subpopulations throughout the loop than there was for

TABLE I. Total dose (D), time period (T), and average dose (D/T) associated with adaptive therapies with antagonistic, additive, and synergistic drug interactions. Antagonistic interactions deliver the smallest total dose over the shortest time period.

e	-0.3	0	0.3
D	118.23	119.42	120.47
T	178.7	192.5	206.7
D/T	0.6616	0.6204	05828

the additive case. Figures 11(e) and 11(f) show an example of an antagonistic $e = -0.3$ adaptive therapy loop. Table I shows the total dose D, time period T, and average dose D/T for each case. The most important takeaway from these numbers is that the antagonistic evolutionary cycle delivers the smallest total dose over the shortest time-period to achieve one closed loop, whereas the synergistic cycle delivers the smallest average dose over the loop, since the time-period is longest.

Figure 12 shows the tumor growth curves for each of the adaptive schedules as compared with the untreated growth curve (exponential growth), and constant therapy curve (each shows tumor regression followed by recurrence). In each case, the adaptive evolutionary cycle overcomes recurrence, with the antagonistic schedule minimizing the tumor regrowth leg (AB) of the schedule.

A final metric that we use for comparisons is the rate of adaptation of the subpopulation i, defined by

$$\alpha_i(t) = \frac{1}{t} \int_0^t x_i(s) \, ds, \qquad (23)$$

which is the time-average of subpopulation level $x_i(t)$. Figure 13 shows the rates of adaptation associated with the two resistant subpopulations R_1 and R_2 during the course of the adaptive schedules. Notice the rate of adaptation is lowest for the antagonistic interaction, which is the main reason the tumor growth curve in Fig. 12(c) is most effective at controlling and delaying tumor recurrence as the cell population evolves.

V. DISCUSSION

The role of synergistic versus antagonistic combination drug interactions on the dynamical balance of coevolving subpopulations of cells is not simple to characterize. In general terms, antagonistic interactions are able to exert a more targeted and subtle range of influences on an evolving population than synergistic ones which, roughly speaking, cause the two-drug combination to effectively act as one. In an coevolutionary setting, this has the effect of enhancing competitive release of resistant cells and more effectively selecting for resistance. Synergistic interactions offer less flexibility for designing effective strategies to manage resistance as the tumor evolves, although might be more beneficial in reducing sensitive cells in static populations. As a byproduct of the ability to deliver a more nuanced control on an evolving population of cells, the sensitivity to small changes in the relative doses of the two drugs in an antagonistic setting seems to be higher than in a synergistic setting (as shown best in Fig. 9). This, perhaps, makes these interactions harder to control.
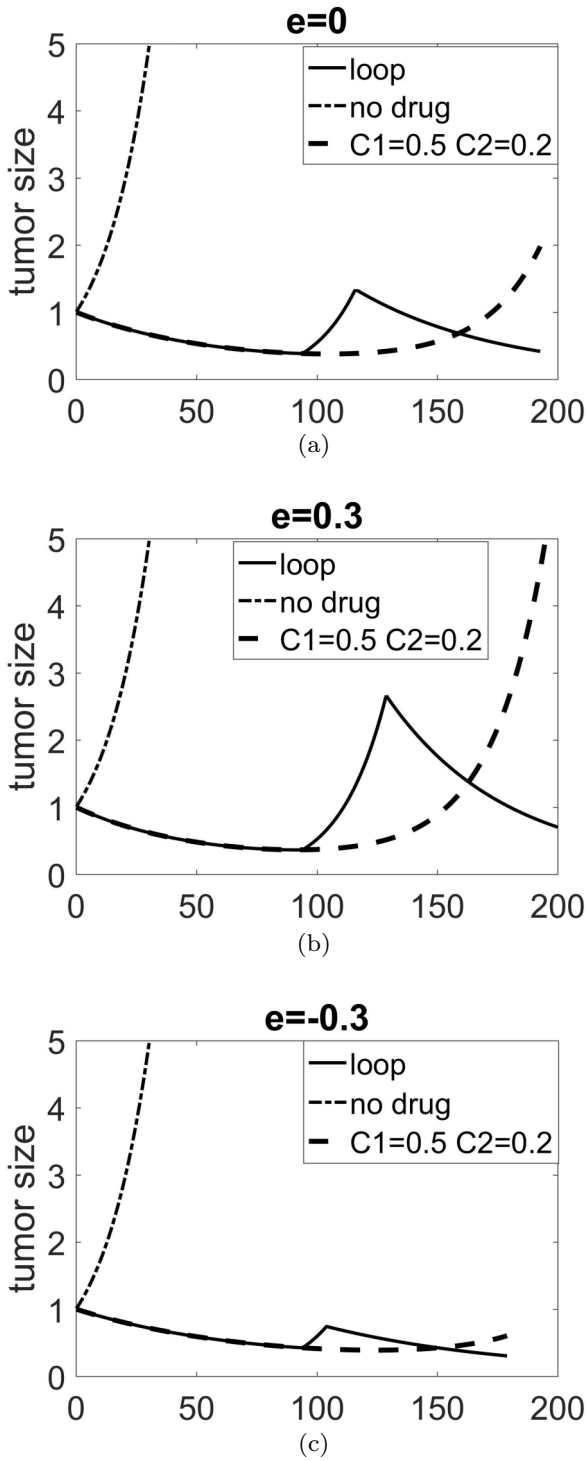
FIG. 12. Tumor growth curves for the adaptive schedules from Fig. 11 as compared with untreated growth (exponential) and constant schedule which eventually leads to tumor recurrence. (a) $e = 0$; (b) $e = 0.3$; (c) $e = -0.3$.

FIG. 13. Rates of adaptation for $e = 0, 0.3, -0.3$: (a) R_1 rate of adaptation; (b) R_2 rate of adaptation.

Tumor recurrence times for the antagonistic drug interactions are delayed more effectively than for synergistic interactions, consistent with the fact that adaptation rates are slower for antagonistic interactions. Antagonistic drug interactions generally provide more flexibility in designing adaptive resistance management schedules.
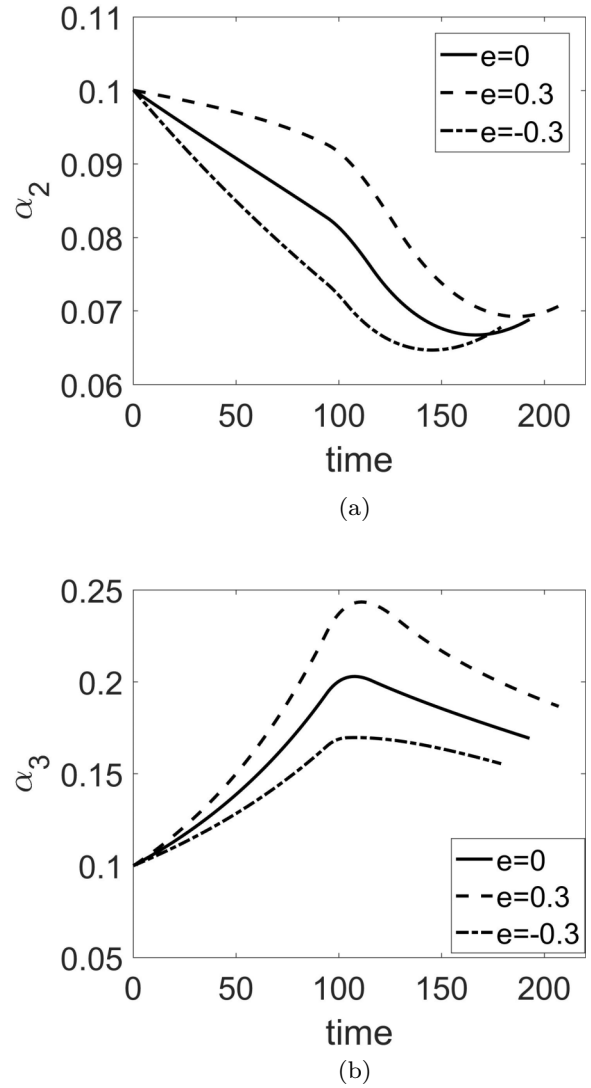
Additional features to our model could be the introduction of mutations that might occur in response to the chemotherapy, which potentially could be handled using a mutational replicator system [29], or a finite-cell Moran process based model [39] to better understand stochastic effects. It might also be possible to analyze existing individual patient data and tumor response curves (as was done in Ref. [41]) to design and optimize better multidrug strategies retrospectively, which is ongoing by our group. There are also ongoing adaptive multidrug clinical trials at the Moffitt Cancer Center that show promise in prostate cancer patients.

[1] P. Newton and Y. Ma, Phys. Rev. E **99**, 022404 (2019).

[2] C. Bliss, Ann. Appl. Biol. **26**, 585 (1939).

[3] S. Loewe, Arzneimittelforschung **3**, 285 (1953).

[4] T. Chou and D. Rideout, *Synergism and Antagonism in Chemotherapy* (Academic Press, NY, 1991).

[5] P. Sudalagunta, M. Silva, R. Canevarolo, R. Gatenby, G. R, R. Baz, M. Meads, K. Shain, and A. Silva, EBioMedicine **54**, 102716 (2020).

[6] A. Read, T. Day, and S. Huijben, Proc. Natl. Acad. Sci. USA **108**, 10871 (2011).

[7] D. Basanta, R. Gatenby, and A. Anderson, Mol. Pharmaceutics **9**, 914 (2012).

[8] R. Gillies, D. Verduzco, and R. Gatenby, Nat. Rev. Cancer **12**, 487 (2012).

[9] R. Gatenby and J. Brown, Cold Spring Harb. Perspect. Med. **8**, a033415 (2018).

[10] J. Zhang, J. Cunningham, J. Brown, and R. Gatenby, Nat. Commun. **8**, 1816 (2017).

[11] J. A. Gallaher, P. M. Enriquez-Navas, K. A. Luddy, R. A. Gatenby, and A. R. Anderson, Cancer Res. **78**, 2127 (2018).

[12] J. West and P. Newton, Cancer Res. **77**, 6717 (2017).

[13] J. West, L. You, J. Zhang, R. Gatenby, J. Brown, P. Newton, and A. Anderson, Cancer Res. **80**, 1578 (2020).

[14] D. Basanta and A. Anderson, Interface Focus **3**, 20130020 (2013).

[15] M. Hegreness, N. Shoresh, D. Damiann, D. Hartl, and R. Kishony, Proc. Natl. Acad. Sci. USA **105**, 13977 (2008).

[16] J. Michel, P. Yeh, R. Chait, R. Moellering, and R. Kishony, Proc. Natl. Acad. Sci. USA **105**, 14918 (2008).

[17] D. Andersson, N. Balaban, F. Baquero, P. Courvalin, P. Glaser, U. Gophna, R. Kishony, S. Molin, and T. Tonjum, FEMS Microbiol. Rev. **44**, 171 (2020).

[18] D. Russ and R. Kishony, Nat. Microbiol. **3**, 1339 (2018).

[19] M. Baym, L. Stone, and R. Kishony, Science **351**, aad3292 (2016).

[20] S. Kim, T. Lieberman, and R. Kishony, Proc. Natl. Acad. Sci. USA **40**, 14494 (2014).

[21] K. Wood, K. Wood, S. Nishida, and P. Cluzel, Cell Rep. **6**, 1073 (2014).

[22] D. Nichol, P. Jeavons, A. Fletcher, R. Bonomo, P. Maini, J. Paul, R. Gatenby, A. Anderson, and J. Scott, PLoS Comput. Biol. **11**, e1004493 (2015).

[23] N. Yoon, R. Vander Velde, A. Marusyk, and J. Scott, Bull. Math. Biol. **80**, 1776 (2018).

[24] M. Lipsitch and B. Levin, Antimicrob. Agents Chemother. **41**, 363 (1997).

[25] I. Bozic and M. Nowak, Proc. Natl. Acad. Sci. USA **111**, 15964 (2014).

[26] S. Hummert, K. Bohl, D. Basanta, A. Deutsch, S. Werner, G. Theiben, A. Schroeter, and S. Schuster, Mol. BioSyst. **10**, 3044 (2014).

[27] K. Bohl, S. Hummert, S. Werner, D. Basanta, A. Deutsch, S. Schuster, G. Theiben, and A. Schroeter, Mol. BioSyst. **10**, 3066 (2014).

[28] J. Hofbauer and K. Sigmund, *Evolutionary Games and Population Dynamics* (Cambridge University Press, Cambridge, UK, 1998).

[29] M. A. Nowak, *Evolutionary Dynamics* (Harvard University Press, Cambridge, MA, 2006).

[30] R. Axelrod, D. E. Axelrod, and K. J. Pienta, Proc. Natl. Acad. Sci. USA **103**, 13474 (2006).

[31] J. West, Z. Hasnain, J. Mason, and P. Newton, Converg. Sci. Phys. Oncol. **2**, 035002 (2016).

[32] D. Andersson and B. Levin, Curr. Opin. Microbiol. **2**, 489 (1999).

[33] I. Bozic and M. Nowak, Ann. Rev. Can. Biol. **1**, 203 (2017).

[34] O. Lavi, M. Gottesman, and D. Levy, Drug Res. Updates **15**, 90 (2012).

[35] N. Komarova and D. Wodarz, Proc. Natl. Acad. Sci. USA **102**, 9714 (2005).

[36] B. Wu, P. M. Altrock, L. Wang, and A. Traulsen, Phys. Rev. E **82**, 046106 (2010).

[37] B. Walsh and M. Blows, Annu. Rev. Ecol. Evol. Syst. **40**, 41 (2009).

[38] J. West and P. Newton, Proc. Natl. Acad. Sci. USA **116**, 1918 (2019).

[39] J. West, Z. Hasnain, P. Macklin, and P. Newton, SIAM Rev. **58**, 716 (2016).

[40] A. Traulsen, J. C. Claussen, and C. Hauert, Phys. Rev. Lett. **95**, 238701 (2005).

[41] J. West, Y. Ma, and P. Newton, J. Theor. Bio. **455**, 249 (2018).

[42] S. Strogatz, *Nonlinear Dynamics and Chaos*, 2nd ed. (Westview Press, Boulder, CO, 2015).

[43] U. Ledzewicz and H. Schattler, J. Optimiz. Theory Appl. **114**, 609 (2002).

[44] W. Koon, M. Lo, J. Marsden, and S. Ross, Chaos **10**, 427 (2000).